Scalable Growth of High-Quality Polycrystalline MoS_2 Monolayers on SiO_2 with Tunable Grain Sizes

Jing Zhang,[†] Hua Yu,[†] Wei Chen,[†] Xuezeng Tian,[†] Donghua Liu,[†] Meng Cheng,[†] Guibai Xie,[†] Wei Yang,[†] Rong Yang,[†] Xuedong Bai,[†,‡] Dongxia Shi,[†] and Guangyu Zhang[†,‡,*]

[†]Beijing National Laboratory for Condensed Matter Physics and Institute of Physics, Chinese Academy of Sciences, Beijing 100190, China and [‡]Collaborative Innovation Center of Quantum Matter, Beijing, China

ABSTRACT We report a scalable growth of monolayer MoS_2 films on SiO_2 substrates by chemical vapor deposition. As-grown polycrystalline MoS_2 films are continuous over the entire substrate surface with a tunable grain size from ~20 nm up to ~1 μm. An obvious blue-shift (up to 80 meV) of photoluminescence peaks was observed from a series samples with different grain sizes. Back-gated field effect transistors based on a polycrystalline MoS_2 film with a typical grain size of ~600 nm shows a field mobility of ~7 $cm^2/(V\ s)$ and on/off ratio of ~10^6, comparable to those achieved from exfoliated MoS_2. Our work provides a route toward scaled-up synthesis of high-quality monolayer MoS_2 for electronic and optoelectronic devices.

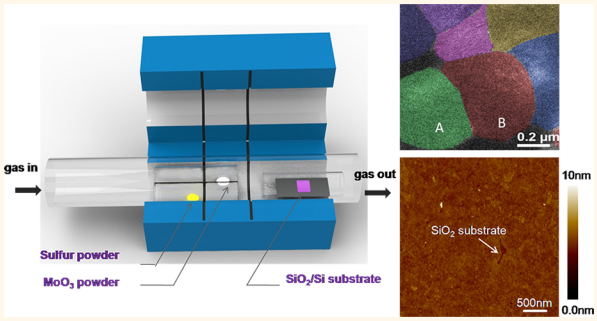

KEYWORDS: MoS_2 · chemical vapor deposition (CVD) · Raman spectrum · photoluminescence · field effect transistor

Monolayer molybdenum disulfide (MoS_2), a direct band gap (E_g = 1.8 eV) semiconductor,[1] shows promise in various electronic and optoelectronic applications.[2−7] From a device point of view, scaled-up fabrication of MoS_2 devices requires large-area, continuous, and high-quality monolayer MoS_2 on a dielectric layer; unfortunately, such materials are currently unavailable. Here we report a scalable growth of polycrystalline monolayer MoS_2 directly on SiO_2 substrates with tunable grain sizes. Band-gap engineering of the polycrystalline MoS_2 monolayer was also demonstrated *via* tuning its grain sizes from tens of nanometers to micrometer scale. The as-grown MoS_2 film fully covers the entire substrate's surface, as evidenced by AFM, Raman, and photoluminescence (PL) imaging. Field effect transistors made of a typical MoS_2 film on SiO_2 with a grain size of ~600 nm show a carrier mobility of ~7 $cm^2/(V\ s)$ and an on/off ratio of ~10^6, revealing the high quality of the material.

Various methods have been developed for scaled-up synthesis of MoS_2 thin layers on insulating substrates. It has been demonstrated that MoS_2 thin layers can be synthesized *via* sulfurization of predeposited Mo thin films or thermal decomposition of $(NH_4)_2MoS_4$ with extra annealing.[8,9] Such methods usually yield multilayer MoS_2 or a mixture of the monolayer and multilayer. Chemical vapor deposition (CVD) is another approach for scaled-up MoS_2 production with sulfur and molybdenum compounds such as MoO_3 and $MoCl_5$ usually used as precursors.[10−15] Large MoS_2 grain size over micrometers has been achieved *via* epitaxial synthesis on a mica surface[16] or growth of highly crystalline triangular islands on SiO_2;[13,14] however, it is still challenging to grow large-scale, continuous, and high-quality MoS_2 films.[16] On the contrary, a continuous MoS_2 film has been grown on sapphire or SiO_2 substrates but with a grain size at the nanometer scale, resulting in a low carrier mobility of less than 1 $cm^2/(V\ s)$.[15]

RESULTS AND DISCUSSION

In this study, we demonstrate the CVD growth of continuous, uniform, and high-quality monolayer MoS_2 directly on a SiO_2 substrate, one of the most used substrates

* Address correspondence to gyzhang@iphy.ac.cn.

Received for review February 25, 2014 and accepted May 12, 2014.

Published online May 12, 2014
10.1021/nn5020819

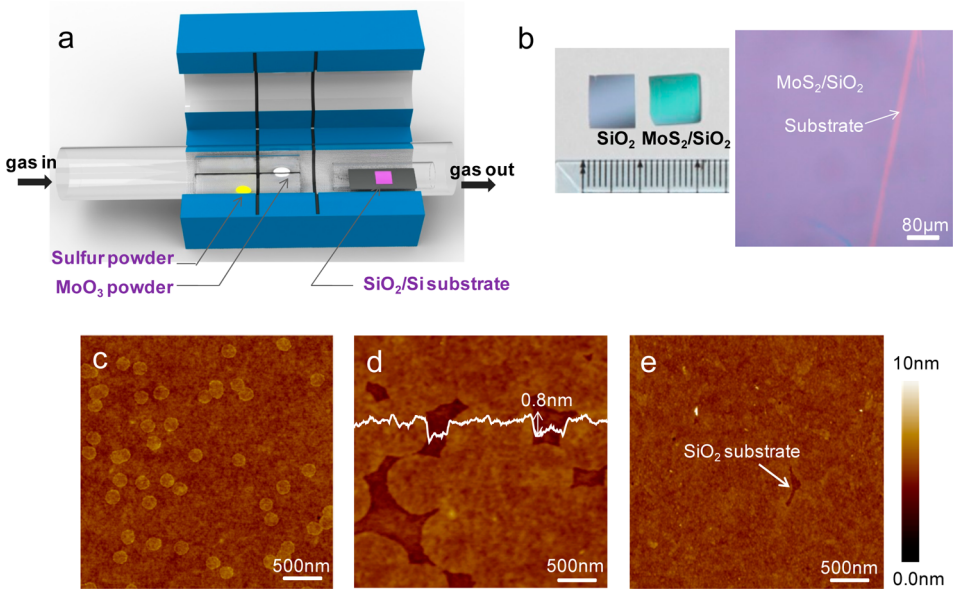

Figure 1. Synthesis setup and morphologies for different synthesis steps. (a) The corresponding locations of sulfur, MoO_3, and SiO_2/Si are indicated in a three-temperature-zone CVD system. (b) Optical photo image contrast between the bare SiO_2/Si substrate and one with CVD grown MoS_2 on it (left). Magnified optical image of as-grown continuous MoS_2 film is shown (right). (c–e) Typical growth steps are indicated by AFM images. The initial MoS_2 nucleation species are shown in (c). The height thickness is plotted in (d). The darker area marked by white arrows indicates the SiO_2 substrate surface in (e).

in semiconductor technology. As depicted in Figure 1a, this CVD setup mainly includes a three-temperature-zone furnace and a 1 in. quartz tube in which sulfur, MoO_3, and substrates were sequentially placed in each temperature zone. Typical temperatures used at zone I (for S), II (for MoO_3), and III (for substrates) are 120–130, 450–600, and 750–800 °C, respectively. The precursor powders were preplaced outside of the furnace and rapidly loaded from outside into each zone for starting the growth. During the growth, argon was used as carrying gas at a flow rate of 130 sccm and the vacuum pressure was kept at 0.67 Torr. Note that the sulfur and MoO_3 sources were separately loaded in two mini-quartz tubes (diameter ~10 mm) in the present design, which provides a stable evaporation of sulfur and MoO_3 sources by avoiding any cross-contaminations during the growth. At the deposition zone, MoO_3 vapor can be reduced in sulfur vapor, eventually leading to a deposition of MoS_2.[10] Figure 1b shows obvious color contrast between photos of a bare substrate and an as-grown sample.[17,18] Zoomed-in optical microscope image of the MoS_2/SiO_2 sample with a scratched strip on the surface is shown on the right in Figure 1b. We can see that monolayer MoS_2 film is uniform and continuous across the entire substrate on a centimeter scale.

The growth of MoS_2 on SiO_2 follows a typical 2D growth mode, *i.e.*, nucleation, growth, and coalescence. Figure 1c–e show atomic force microscope (AFM) images of a series of samples after growth for 15, 25, and 50 min. For all these growths, 130, 540, and 750 °C were used for zones I, II, and III, respectively, and the amounts of sulfur/MoO_3 powders were fixed at 0.6 g/35 mg. We can see that, at the early stage of growth, MoS_2 nuclei were randomly distributed on the SiO_2 surface (Figure 1c). With growth continuing, these nuclei grow into larger grains (Figure 1d), and eventually, a continuous film can be formed by coalescence (Figure 1e). The thickness of these grains or continuous film is ~0.8 nm (as seen in the height profile cut along the white line in Figure 1d), equal to a monolayer thickness of MoS_2. The MoS_2 grain size in Figure 1e is ~600 nm. The AFM height images of the as-grown film show uniform color contrast, suggesting the homogeneous thickness of monolayer MoS_2.

From Figure 1c–e, we can see that only monolayer MoS_2 was grown; bilayer or multilayer MoS_2 was rarely seen. Such self-terminated growth is in agreement with previous observations.[15] It is also worth noting that the nucleation process occurs only at the early growth of stage and is likely to stop afterward, as evidenced from the uniform sizes of the enlarged grains. This phenomenon can be understood from a thermodynamics point of view. For 2D materials nucleation, steady nuclei form at the defect sites on a surface. With increased nuclei density, incoming MoS_2 species need to diffuse only comparatively shorter distance to coalesce into the nuclei already formed rather than initiating new ones. Amounts of these metastable nuclei obey the rule called "detailed balance",[24] and smaller grains can be turned into larger ones by adsorbing atoms, while larger grains become smaller by releasing some atoms. Thus, at the thermodynamic equilibrium point, each grain keeps a homogeneous size. Moreover, the mean free diffusion length of incoming MoS_2 species on SiO_2 is expected to be

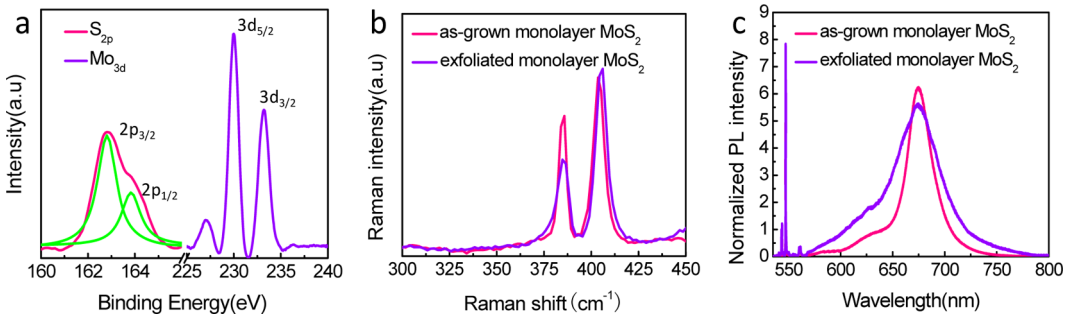

Figure 2. Optical characterizations of a continuous monolayer MoS_2 atomic layer. (a) X-ray photoemission spectroscopy (XPS) demonstrating binding energy for Mo and S. (b, c) Typical Raman and normalized PL spectrum comparisons between our as-grown monolayer MoS_2 thin film and an exfoliated one.

much shorter than that on MoS_2. As a result, growth is favored on the SiO_2 surface rather than as nucleated MoS_2 species until the SiO_2 surface is fully covered.

In order to further study the MoS_2 structure of the as-grown continuous films, we carried out optical characterizations (Figure 2). X-ray photoelectron spectroscopy (XPS) of the sample (Figure 2a) reveals the existence of Mo^{4+}, peaking at 230 eV ($3d_{5/2}$) and 233.2 eV ($3d_{3/2}$), and S^{2-}, peaking at 162.7 eV ($2p_{3/2}$) and 163.8 eV ($2p_{1/2}$), with an atomic composition ratio for S and Mo of 2:1. This sample was also characterized by Raman (Figure 2b) and photoluminescence spectroscopy (Figure 2c) with 532 nm excitation laser. As a comparison, exfoliated monolayer MoS_2 on SiO_2 was also included as control samples. According to the literature,[19−21] Raman peaks at 386.5 and 406.3 cm^{-1} (Figure 2b) correspond to in-plane vibration of Mo and S atoms (E_{2g} mode) and out-of-plane vibration of the S atom (A_{1g} mode), respectively. Spacing between the two peaks (Δ) is ~19.8 cm^{-1}, which is close to exfoliated monolayer MoS_2 (Δ = 19.4 cm^{-1}). The full width at half-maximum (fwhm) of E_{2g}, ~5.1 cm^{-1}, confirms the monolayer nature and high quality of the as-grown MoS_2 as compared with the exfoliated one. The PL spectrum of the sample is also very similar to that of exfoliated MoS_2 (Figure 2c), with two characteristic peaks at 625 nm (B_1 excitation, originating from the valence band splitting caused by strong spin−obit coupling) and 675 nm (A_1 excitation, derived from direct band gap).[22,23] The PL peaks were normalized to the intensity of the Raman A_{1g} peak to rule out other external factors.[22] The normalized PL intensity exceeding 6 is more evidence of the high quality of the sample. Note that the observed PL fwhm for our synthesized monolayer MoS_2 is much smaller than the exfoliated one, indicating a high crystal quality. More details of Raman and PL mapping images for as-grown monolayer MoS_2 are provided in the Supporting Information (Figure S1).

Transmission electron microscopy (TEM) was also applied to confirm the atomic structure of the as-grown MoS_2 film. Figure 3a is the typical bright-field TEM (BF-TEM) image showing the morphology of the continuous MoS_2 thin film. The folded edge in Figure 3b reveals that our MoS_2 film is monolayer. The high-resolution TEM image in Figure 3c confirms the defect-free honeycomb lattice arrangement of MoS_2 with typical (100) and (110) interplanar spacings of 0.27 and 0.16 nm, respectively. Dark-field TEM (DF-TEM) can characterize the grain boundary and the grain size in polycrystalline MoS_2 films.[13,14] The DF-TEM brightness contrast in Figure 3d reveals that individual grains (marked with A and B) are single crystalline, while for the continuous MoS_2 film formed by grain−grain coalescence, grain boundaries are expected since these grains on SiO_2 have a random distribution of lattice orientations. Figure 3e shows the corresponding false-color DF-TEM image constructed by overlaying different DF-TEM images. A grain with uniform color is single crystalline, while grains with different colors reveal different lattice orientations. For two adjacent MoS_2 grains, the selected-area electron diffraction (SAED) pattern covering the grain boundary marked with a yellow dashed circle shows two sets of 6-fold symmetry crystal structures with a 25° orientation difference (Figure 3f). Note that we can rarely see bilayers or a disconnect gap between two adjacent grains. This is consistent with the results shown in Figure 1d and e. In addition, the typical grain size in the polycrystalline MoS_2 film shown in Figure 3e can be confirmed to be ~600 nm.

As-grown MoS_2 films on 300 nm SiO_2 substrates with a typical grain size of ~600 nm were also used for fabrication of back-gated field effect transistor (FET) devices. The film was first patterned into strips by electron beam lithography (EBL) and Ar-plasma etching; Ti/Au (2 nm/40 nm) contact electrodes were then defined by additional EBL, metal evaporation, and a lifting-off process. Devices were annealed at 380 °C for 1 h in an argon atmosphere before electrical measurements in a vacuum with a base pressure of $<2 \times 10^{-7}$ Pa. Figure 4a shows an optical image of typical devices. The transfer and output characteristics of a device with channel length L = 20 μm and channel width W = 5 μm are shown in Figure 4b and c, respectively. These devices show typical n-type behavior with a

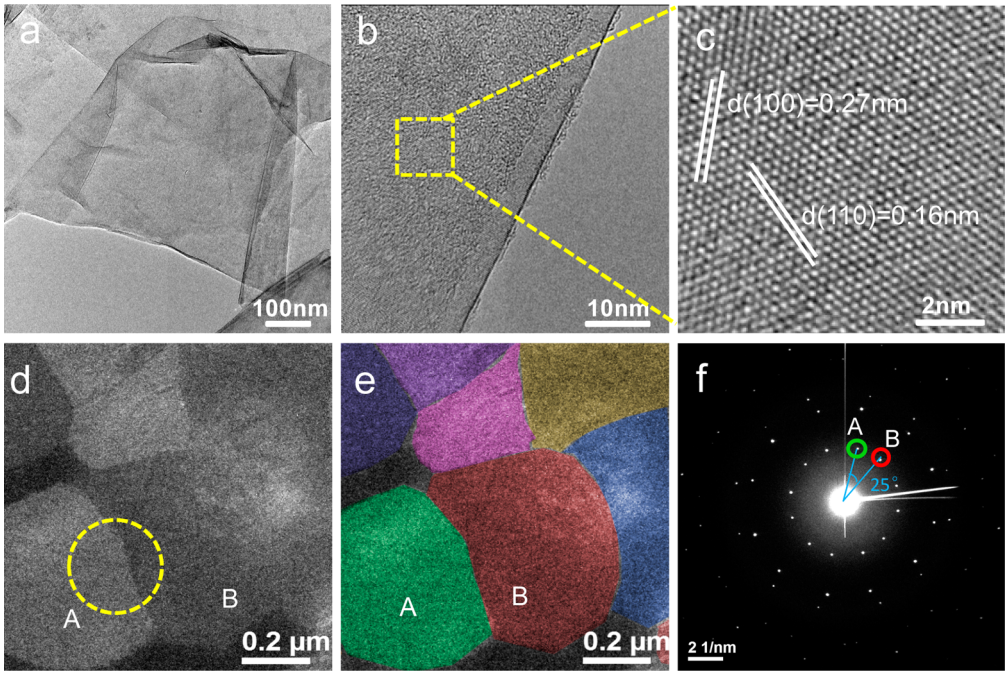

Figure 3. TEM characterizations of a 600 nm grain-sized MoS_2 thin film. (a) Bright-field (BF) TEM image of a MoS_2 thin film. (b) BF-TEM image of as-grown monolayer MoS_2 with a folded edge. (c) The HR-TEM image magnified from the area marked with a yellow square shows a crystalline orientation. The (100) and (110) interplanar spacing is 0.27 and 0.16 nm, respectively. (d) Dark-field TEM image presenting different crystal orientation and grain size. (e) Corresponding false-color DF-TEM of (d). Grains A and B colored with green and red confirm two adjacent single-crystalline MoS_2 flakes coalescence with random orientation. (f) Corresponding SAED pattern for the area marked with a yellow dashed circle in Figure 3d.

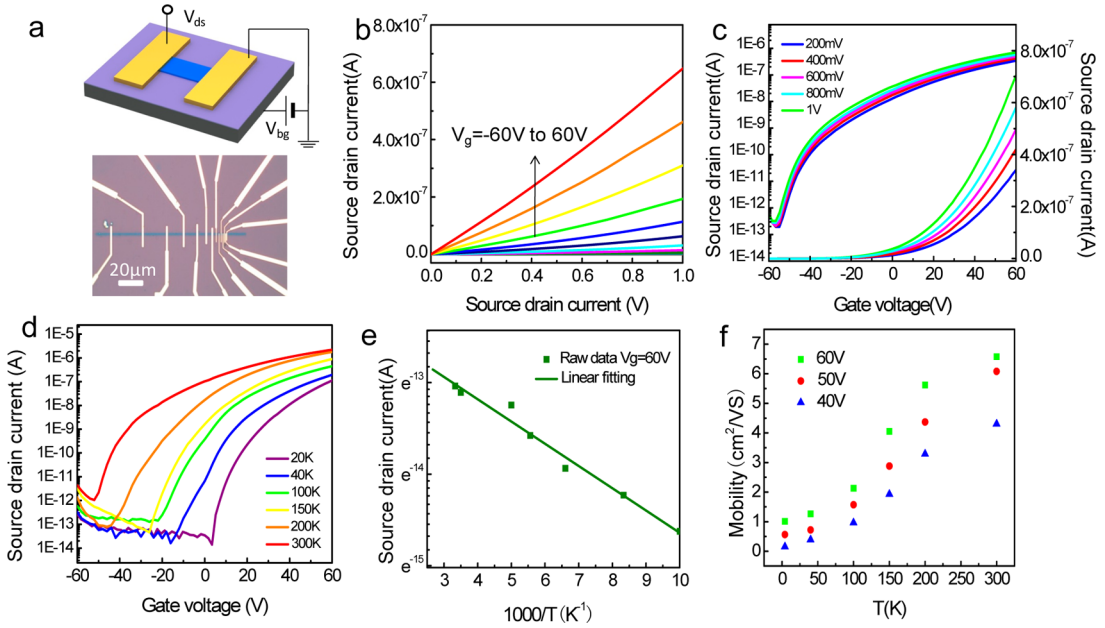

Figure 4. Electrical properties of an as-grown monolayer MoS_2 film. (a) The device schematic diagram is shown (top). The optical image shows the as-fabricated FET device with various channel lengths based on as-grown monolayer MoS_2 with a 600 nm domain size (bottom). (b, c) Electrical output and transfer curve of this device. Back-gate voltage (V_g) sweeping: −60 to 60 V; source−drain bias (V_{ds}): 200 mV to 1 V. (d) Transfer curve for the device when reducing the temperature from 300 K to 20 K. (e) The temperature dependence of source−drain current is plotted using the thermally activated transport model. (f) The statistical mobility as a function of temperature is shown at 40, 50, and 60 V gate voltage.

maximum on/off ratio of more than 5×10^6 at 300 K. The threshold voltage is at −50 V. We calculated the electron mobility of MoS_2 in this device using a standard transistor model,[25−28] and the resulting mobility is 7 ± 0.5 cm^2/(V s), which is very close to the number obtained previously from exfoliated MoS_2 on SiO_2 (0.1−10 cm^2/(V s)).[2] (Other electrical measurement results are shown in Figures S2 and S3.)

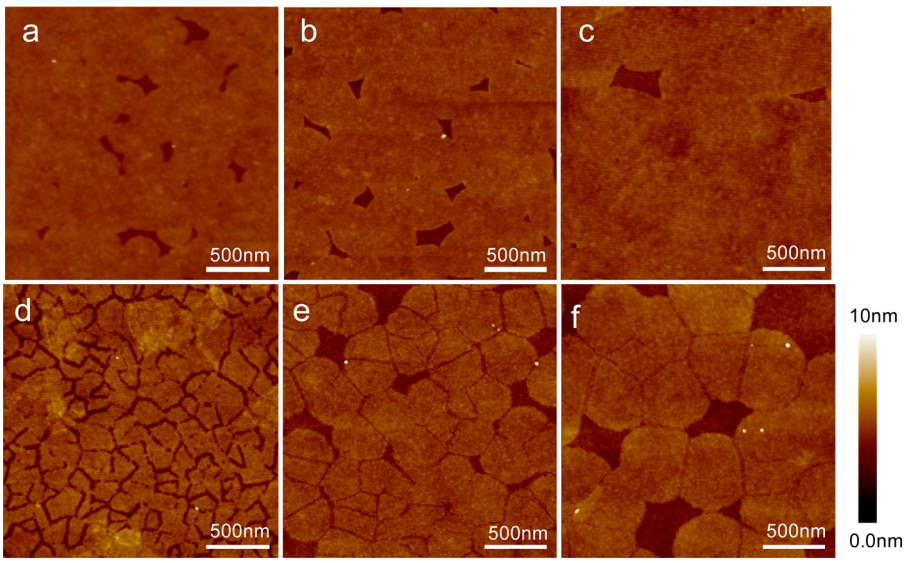

Figure 5. AFM images of MoS_2 continuous thin films with 200, 400, and 600 nm grain size before and after O_2 treatments. (a–c) Typical AFM images for 200, 400, and 600 nm grain-sized MoS_2 thin film. (d–f) Corresponding AFM images after oxidation at 250 °C for 15 min.

We also carried out cool-down measurements for the same device. Figure 4d shows the typical transfer curve at various temperatures. An obvious threshold voltage shift from −50 V to 0 V was observed during cooling from 300 K to 20 K, indicating a suppression of the substrate doping effect. Off-state drain currents show an obvious decrease during cooling. For the monolayer MoS_2 device, I_{ds} dependence of temperature can be explained by the model of thermally activated transport. From these transfer curves, we can estimate thermal activation energy E_a based on the thermally activated transport formula:[29] $I_{ds} = V_{ds}G_0(T)\, e^{-E_a/k_BT}$, where I_{ds} (V_{ds}) is the source–drain current (voltage), $G_0(T)$ is the temperature (T)-related parameter, and k_B is the Boltzmann constant. The curve of ln I_{ds} *versus* $1/T$ is plotted at fixed V_{ds} in Figure 4e. From a linear fitting, we can extract an E_a of ~0.2 eV, which is much smaller than the band gap of monolayer MoS_2. This can be attributed to the depth of the donor band located above the valence band caused by impurities or defects.[1,23] We also plotted the mobility as a function of temperature at V_g = 40, 50, and 60 V (Figure 4f). We can see that the overall mobility is higher at higher V_g, and at the fixed V_g, the mobility decreases with temperature. In this case, charge impurities scattering is the dominant factor that limits the mobility.

As discussed above, DF-TEM is useful for directly viewing the grain sizes and grain boundaries in the as-grown MoS_2 films. However, it is not convenient when dealing with large-scale samples. Thus, we developed an easy and fast approach to identify the grain boundaries in our MoS_2 films. This approach includes, first, calcining in air and, second, imaging *via* AFM. Grain boundaries are usually invisible under AFM imaging, but they may become visible after calcinations since these grain boundaries are preferred sites for etching. Figure 5a–c show typical AFM images of three as-grown samples with different grain sizes. After calcining in air at 250 °C for 15 min, grain boundaries were etched, resulting in etched grooves in the MoS_2 films (Figure 5d–f). The average grain sizes of the three samples are estimated to be ~200, ~400, and ~600 nm, respectively. In this way, the information on grain boundaries and sizes can be easily obtained, which is also consistent with our TEM characterizations.

As seen above, as-grown continuous, monolayer, large grain sized MoS_2 on SiO_2 is of high quality, close to that of exfoliated MoS_2. It is also interesting, but rarely reported, to investigate the band-gap engineering in such polycrystalline films. By controlling the amount and evaporation temperature of the precursors, the deposition temperature of the substrate, and growth duration, we are able to grow a series of MoS_2 samples (#1–6) with various grain sizes (the topography of the AFM images is provided in Supporting Information Figure S4). The average grain sizes of samples #1–6 were estimated from the approach described above. Figure 6a shows the Raman spectra of samples #1–6, revealing very similar features in terms of peak positions and intensity. However, PL spectra of these samples differ obviously, and a blue shifting was observed when the grain size decreases from ~100 nm to ~20 nm (Figure 6b). We can see that the band gap of the samples can be tuned from 1.84 eV to 1.92 eV reliably (80 meV blue-shift for the peak position of A_1 excitation). No obvious blue-shifting of energy (<10 meV) was observed when the grain size increases to over 100 nm. We attributed this upshift of peak energy to the varied grain boundary density, as the local change of doping or strain around the grain

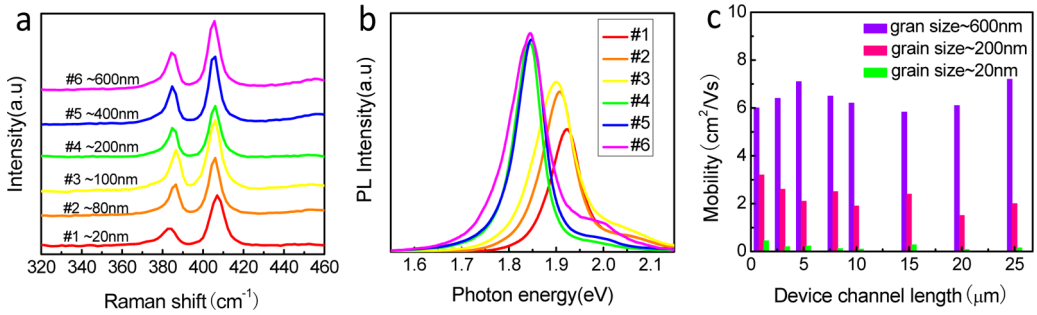

Figure 6. A series of continuous MoS_2 samples with different domain sizes show obvious energy blue-shift caused by various domain boundary density. (a) Raman spectra for a series of samples marked #1 to #6 with various domain sizes from 20 to 600 nm. (b) Photoluminescence shift for corresponding samples from #1 to #6. (c) Statistics data of mobility as a function of channel length based on monolayer MoS_2 transistors with grain sizes of 20, 200, and 600 nm, respectively (corresponding AFM images for samples #1 to #6 are shown in Supporting Information Figure S4).

boundary may modulate the band structure.[13,14,30−32] Note that the laser spot size performed for the PL spectra is about 1 μm, which is larger than the grain size in all our samples.

Moreover, we also investigated the electrical property of continuous MoS_2 films with varied grain sizes. The distribution of mobility with MoS_2 grain sizes of ~600, ~200, and ~20 nm is plotted as a function of varied channel length in Figure 6c. We can clearly see that films with smaller grains have lower mobility. For a typical 20 nm MoS_2 film, the mobility is less than 0.5 $cm^2/(V\ s)$. This is expected since smaller grains would lead to extra scattering for electron transport in the polycrystalline MoS_2 film,[14,15] while for 200 and 600 nm MoS_2 films, the mobility ranges from 2 to 7 $cm^2/(V\ s)$, indicating that grain boundary plays a limited role in the carrier transport through polycrystalline MoS_2 films.

CONCLUSION

We developed a facile method to grow centimeter-scale, continuous, and uniform monolayer MoS_2 films *via* a new CVD configuration. The growth of MoS_2 thin films on SiO_2 follows a typical 2D growth mode: nucleation, growth, and coalescence. As-grown films are of high quality comparable to exfoliated MoS_2, as evidenced from Raman, PL, HRTEM, and also electrical transport characterizations. We also demonstrate the possibility of band-gap engineering in such polycrystalline films by tailoring the grain sizes. Our work suggests that these scalable CVD MoS_2 films are ideal materials for electronic and optoelectronic devices.

METHODS

Growth of MoS_2 Films. The MoS_2 film was grown on a SiO_2 (300 nm)/p++Si substrate precleaned with acetone and 2-propanol. The growth process was carried out in a CVD system using MoO_3 (Alfa Aesar 99.999%) and S (Alfa Aesar 99.9%) powder as the precursor. Typical designed lengths used at zones I (for S), II (for MoO_3), and III (for substrates) are 15, 10, and 20 cm, respectively. The length of the heat insulating layer between each temperature zone is 10 cm. The distance between S and MoO_3 is 22 cm. The SiO_2 substrates were placed downwind along zone III. The typical length between MoO_3 and SiO_2 for continuous MoS_2 monolayer growth is 18 cm. The tunable growth parameters include precursor evaporation temperature, substrate deposition temperature, pressure, gas flow rate, the relative location of SiO_2/Si, growth duration, *etc.* Each of the three temperature zones was heated to a preset value at a rate of 25 °C/min, respectively. Each temperature zone was kept stable for 20 min before growth.

Fabrication of the MoS_2 FET Devices. The 5% 495 PMMA in anisole was spin-coated at 4000 rpm on the as-prepared samples and then was patterned into strips by a Raith e-beam lithography system (or optical lithography). Argon-plasma etching as reactive gas was carried out in a reactive ion etching system (PlasmaLab 80 Plus, Oxford Instruments Company). The plasma power, argon pressure, flow rate, and etching time are 50 W, 0.1 Torr, 50 sccm, and 20 s, respectively. Metal electrodes were then made for the patterned MoS_2 by electron beam lithography, metal film deposition, and lifting-off techniques. Electrical measurements were performed with an Agilent semiconductor parameter analyzer (4156C) under high vacuum in a four-probe station system.

Characterizations of As-Grown MoS_2 Film. Raman spectroscopy was carried out using a Horiba Jobin Yvon LabRAM HR-Evolution Raman microscope. The excitation light is a 532 nm laser, with an estimated laser spot size of 1 μm and a laser power of 10 mW. High-resolution Raman and photoluminescence mapping images were obtained with a 100× objective, 600 grooves/mm grating, and a 500 nm mapping step. The surface morphology images of MoS_2 were characterized by an atomic force microscope (AFM, MultiMode IIId, Veeco Instruments Inc.) Elemental composition analysis was performed using X-ray photoelectron spectroscopy (ESCALAB 250, Thermo Fisher Scientific Inc.) with focused monochromatized Al Ka radiation. Transmission electron microscopy images were performed at 200 kV in a JEOL 2010F field-emission-type high-resolution TEM. For TEM characterizations, the as-grown monolayer MoS_2 was transferred to a TEM grid by etching away the SiO_2 with hydrofluoric acid solution.

Conflict of Interest: The authors declare no competing financial interest.

Acknowledgment. This work was supported by the National Basic Research Program of China (973 Program, grant nos. 2013CB934500 and 2012CB921302), the National Science Foundation of China (NSFC, grant nos. 91223204, 61325021, 11204358, and 11174333), and the Chinese Academy of Sciences.

Supporting Information Available: More Raman and photoluminescence mapping images of as-grown MoS_2 films and more AFM images and electrical measurements for MoS_2 films with varied grain sizes. This material is available free of charge *via* the Internet at http://pubs.acs.org.

REFERENCES AND NOTES

1. Mak, K. F.; Lee, C.; Hone, J.; Shan, J.; Heinz, T. F. Atomically Thin MoS_2: A New Direct-Gap Semiconductor. *Phys. Rev. Lett.* **2010**, *105*, 136805.
2. Radisavljevic, B.; Radenovic, A.; Brivio, J.; Giacometti, V.; Kis, A. Single-Layer MoS_2 Transistors. *Nat. Nanotechnol.* **2011**, *6*, 147–150.
3. Ghatak, S.; Pal, A. N.; Ghosh, A. Nature of Electronic States in Atomically Thin MoS_2 Field-Effect Transistors. *ACS Nano* **2011**, *5*, 7707–7712.
4. Baugher, B. W. H.; Churchill, H. O. H.; Yang, Y. F.; Jarillo-Herrero, P. Intrinsic Electronic Transport Properties of High-Quality Monolayer and Bilayer MoS_2. *Nano Lett.* **2013**, *13*, 4212–4216.
5. Radisavljevic, B.; Whitwick, M. B.; Kis, A. Integrated Circuits and Logic Operations Based on Single-Layer MoS_2. *ACS Nano* **2011**, *5*, 9934–9938.
6. Yin, Z. Y.; Li, H.; Li, H.; Jiang, L.; Shi, Y. M.; Sun, Y. H.; Lu, G.; Zhang, Q.; Chen, X. D.; Zhang, H. Single-Layer MoS_2 Phototransistors. *ACS Nano* **2012**, *6*, 74–80.
7. Lee, H. S.; Min, S. W.; Chang, Y. G.; Park, M. K.; Nam, T.; Kim, H.; Kim, J. H.; Ryu, S.; Im, S. MoS_2 Nanosheet Phototransistors with Thickness-Modulated Optical Energy Gap. *Nano Lett.* **2012**, *12*, 3695–3700.
8. Zhan, Y. J.; Liu, Z.; Najmaei, S.; Ajayan, P. M.; Lou, J. Large-Area Vapor-Phase Growth and Characterization of MoS_2 Atomic Layers on a SiO_2 Substrate. *Small* **2012**, *8*, 966–971.
9. Liu, K. K.; Zhang, W. J.; Lee, Y. H.; Lin, Y. C.; Chang, M. T.; Su, C.; Chang, C. S.; Li, H.; Shi, Y. M.; Li, L. J. Growth of Large-Area and Highly Crystalline MoS_2 Thin Layers on Insulating Substrates. *Nano Lett.* **2012**, *12*, 1538–1544.
10. Lee, Y. H.; Zhang, X. Q.; Zhang, W. J.; Chang, M. T.; Lin, C. T.; Chang, K. D.; Yu, Y. C.; Chang, C. S.; Li, L. J.; Lin, T. W. Synthesis of Large-Area MoS_2 Atomic Layers with Chemical Vapor Deposition. *Adv. Mater.* **2012**, *24*, 2320–2325.
11. Lin, Y. C.; Zhang, W. J.; Huang, J. K.; Liu, K. K.; Lee, Y. H.; Liang, C. T.; Chu, C. W.; Li, L. J. Wafer-Scale MoS_2 Thin Layers Prepared by MoO_3 Sulfurization. *Nanoscale* **2012**, *4*, 6637–6641.
12. Balendhran, S.; Ou, J. Z.; Bhaskaran, M.; Sriram, S.; Ippolito, S.; Vasic, Z.; Kats, E.; Bhargava, S.; Zhuiykov, S.; Kalantar-zadeh, K. Atomically Thin Layers of MoS_2 via a Two Step Thermal Evaporation-Exfoliation Method. *Nanoscale* **2012**, *4*, 461–466.
13. Najmaei, S.; Liu, Z.; Zhou, W.; Zou, X. L.; Shi, G.; Lei, S. D.; Yakobson, B. I.; Idrobo, J. C.; Ajayan, P. M.; Lou, J. Vapour Phase Growth and Grain Boundary Structure of Molybdenum Disulphide Atomic Layers. *Nat. Mater.* **2013**, *12*, 754–759.
14. van der Zande, A. M.; Huang, P. Y.; Chenet, D. A.; Berkelbach, T. C.; You, Y. M.; Lee, G. H.; Heinz, T. F.; Reichman, D. R.; Muller, D. A.; Hone, J. C. Grain and Grain Boundaries in Highly Crystalline Monolayer Molybdenum Disulphide. *Nat. Mater.* **2013**, *12*, 554–561.
15. Yu, Y. F.; Li, C.; Liu, Y.; Su, L. Q.; Zhang, Y.; Cao, L. Y. Controlled Scalable Synthesis of Uniform, High-Quality Monolayer and Few-Layer MoS_2 Films. *Sci. Rep.* **2013**, *3*, 1866–1871.
16. Ji, Q. Q.; Zhang, Y. F.; Gao, T.; Zhang, Y.; Ma, D. L.; Liu, M. X.; Chen, Y. B.; Qiao, X. F.; Sun, Q.; Liu, Z. F. Epitaxial Monolayer MoS_2 on Mica with Novel Photoluminescence. *Nano Lett.* **2013**, *13*, 3870–3877.
17. Castellanos-Gomez, A.; Agrait, N.; Rubio-Bollinger, G. Optical Identification of Atomically Thin Dichalcogenide Crystals. *Appl. Phys. Lett.* **2010**, *96*, 213116.
18. Benameur, M. M.; Radisavljevic, B.; Heron, J. S.; Sahoo, S.; Berger, H.; Kis, A. Visibility of Dichalcogenide Nanolayers. *Nanotechnology* **2011**, *22*, 125706.
19. Lee, C.; Yan, H.; Brus, L. E.; Heinz, T. F.; Hone, J.; Ryu, S. Anomalous Lattice Vibrations of Single- and Few-Layer MoS_2. *ACS Nano* **2010**, *4*, 2695–2700.
20. Molina-Sanchez, A.; Wirtz, L. Phonons in Single-Layer and Few-Layer MoS_2 and WS_2. *Phys. Rev. B* **2011**, *84*, 155413.
21. Najmaei, S.; Liu, Z.; Ajayan, P. M.; Lou, J. Thermal Effects on the Characteristic Raman Spectrum of Molybdenum Disulfide (MoS_2) of Varying Thicknesses. *Appl. Phys. Lett.* **2012**, *100*, 013106.
22. Splendiani, A.; Sun, L.; Zhang, Y. B.; Li, T. S.; Kim, J.; Chim, C. Y.; Galli, G.; Wang, F. Emerging Photoluminescence in Monolayer MoS_2. *Nano Lett.* **2010**, *10*, 1271–1275.
23. Eda, G.; Yamaguchi, H.; Voiry, D.; Fujita, T.; Chen, M. W.; Chhowalla, M. Photoluminescence from Chemically Exfoliated MoS_2. *Nano Lett.* **2012**, *12*, 526–526.
24. Venables, J. A.; Spiller, G. D. T.; Hanbucken, M. Nucleation and Growth of Thin-Films. *Rep. Prog. Phys.* **1984**, *47*, 399–459.
25. Yoon, Y.; Ganapathi, K.; Salahuddin, S. How Good Can Monolayer MoS_2 Transistors Be? *Nano Lett.* **2011**, *11*, 3768–3773.
26. Pu, J.; Yomogida, Y.; Liu, K. K.; Li, L. J.; Iwasa, Y.; Takenobu, T. Highly Flexible MoS_2 Thin-Film Transistors with Ion Gel Dielectrics. *Nano Lett.* **2012**, *12*, 4013–4017.
27. Liu, H.; Neal, A. T.; Ye, P. D. D. Channel Length Scaling of MoS_2 MOSFETs. *ACS Nano* **2012**, *6*, 8563–8569.
28. Das, S.; Chen, H. Y.; Penumatcha, A. V.; Appenzeller, J. High Performance Multilayer MoS_2 Transistors with Scandium Contacts. *Nano Lett.* **2013**, *13*, 100–105.
29. Radisavljevic, B.; Kis, A. Mobility Engineering and a Metal-Insulator Transition in Monolayer MoS_2. *Nat. Mater.* **2013**, *12*, 815–820.
30. Mak, K. F.; He, K. L.; Lee, C.; Lee, G. H.; Hone, J.; Heinz, T. F.; Shan, J. Tightly Bound Trions in Monolayer MoS_2. *Nat. Mater.* **2013**, *12*, 207–211.
31. Conley, H. J.; Wang, B.; Ziegler, J. I.; Haglund, R. F., Jr.; Pantelides, S. T.; Bolotin, K. I. Bandgap Engineering of Strained Monolayer and Bilayer MoS_2. *Nano Lett.* **2013**, *13*, 3626–3230.
32. Scalise, E.; Houssa, M.; Pourtois, G.; Afanas'ev, V. V.; Stesmans, A. Strain-Induced Semiconductor to Metal Transition in the Two-Dimensional Honeycomb Structure of MoS_2. *Nano Res.* **2012**, *5*, 43–48.